Micro-sized Si-C Composite with Interconnected Nanoscale Building Blocks as High-Performance Anodes for Practical Application in Lithium-Ion Batteries

*Ran Yi, Fang Dai, Mikhail L. Gordin, Shuru Chen, and Donghai Wang**

The emerging markets of electric vehicles (EV) and plug-in hybrid electric vehicles (PHEV) generate a tremendous demand for low-cost lithium-ion batteries (LIBs) with high energy and power densities and long cycling life.[1–4] The development of such LIBs requires development of low cost, high energy-density cathode and anode materials. Conventional anode materials in commercial LIBs are primarily synthetic graphite-based materials with a capacity of ~370 mAh/g.[5] Improvements in anode performance, particularly in anode capacity, are essential to achieving high energy densities in LIBs for EV and PHEV applications.

Silicon has been intensively pursued as the most promising anode material for high-energy-density LIBs because of its high specific capacity (>3500 mAh/g) and abundance.[6] Despite its high capacity, Si suffers from fast capacity fading caused by its large volume change (>300%) during lithiation/delithiation and the serious issues stemming from this volume change, e.g., unstable solid electrolyte interphase (SEI) and disintegration (cracking and crumbling) of the electrode structure.[7,8] The development of Si-C nanocomposites (e.g., nanowires, nanotubes, or nanoparticles) has been widely studied.[9–18] These nanocomposites proved to be an effective method of improving capacity and cycling stability, since nano-sized Si can alleviate fracture during volume changes and the contact between Si and carbon can maintain electrical contact and improve conductivity of the nanocomposites. However, practical application of nano-sized Si materials in LIBs is difficult. First, achieving a high tap density is important for fabrication of high-energy LIBs for EVs and PHEVs, because it offers a high volumetric energy density. Unfortunately, the tap density of nano-sized materials is generally low, which in turn holds down their volumetric capacity.[19] Furthermore, preparation of nano-sized Si either requires chemical/physical vapor deposition or involves complicated processes, leading to costly, low-yield synthesis that is difficult to scale up to practical levels.[20–22] To date, the abundance of Si has not been fully capitalized upon due to lack of a low-cost strategy for large-scale synthesis of Si anode materials with superior performance.

Micro-sized materials are favorable for practical battery applications since they often enable higher tap density than nano-sized materials and, as a result, are expected to offer higher volumetric capacity.[23,24] However, the disadvantages of micro-sized Si materials as anodes are obvious. Micro-sized Si particles are more likely to undergo disintegration upon volume change during lithiation/delithiation compared with nano-sized materials, resulting in severe capacity fading.[25] Micro-sized materials also have long ion/electron transport paths that adversely affect high rate capability.[23] Because of these trade-offs, it is desirable to develop new materials that combine the advantages of both micro-sized and nano-sized Si materials to improve the cycling performance, rate capability, and energy density of Si anodes.

Such micro-sized Si anode materials with nanoscale building blocks have been previously demonstrated with encouraging results. Cho et al. developed a porous Si-C composite with a nanocrystalline Si framework by a templating approach.[26] The porous Si-C shows excellent electrochemical performance with high capacity and good cycling stability, due to volume change accommodation by its pores. A low cost approach was reported by Cho and Park et al. to produce micro-sized porous Si-C composites by catalytically etching surface layers of micro-sized Si followed by carbon coating.[27,28] The obtained micro-sized porous Si-C powder shows good cycling stability within the limited number of cycles tested (less than 70 cycles). Yushin et al. reported another type of micro-sized porous C–Si nanocomposite, prepared by physically depositing Si nanoparticles into porous micro-sized carbon granules, which exhibits high capacity and good capacity retention.[29] The micro-sized porous C-Si material has a tap density of 0.49 cm^3/g and high volumetric capacity of 1270 mAh/cm^3 at a current density of 149 mA/g. Micro-sized, carbon-coated Si-based multicomponent anodes composed of Si/SiO cores and crystalline SiO_2 shells were developed by Park et. al. and show a high reversible capacity and good capacity retention.[30] However, between these and other reports, there are still few low-cost and scalable approaches for preparing micro-sized Si-C composite anodes with high energy density as well as good cycling and rate performance.

Inspired by the previous findings, we propose that micro-sized Si-C composites should have the following features to obtain excellent electrochemical performance: 1) the size of primary Si building blocks should be small enough to avoid building block fracture induced by volume changes during the

R. Yi,[+] Dr. F. Dai,[+] M. L. Gordin, S. Chen, Prof. D. Wang
Department of Mechanical and Nuclear Engineering
The Pennsylvania State University
University Park, PA 16802, USA
E-mail: dwang@psu.edu
[+] These authors contributed equally to this work

DOI: 10.1002/aenm.201200857

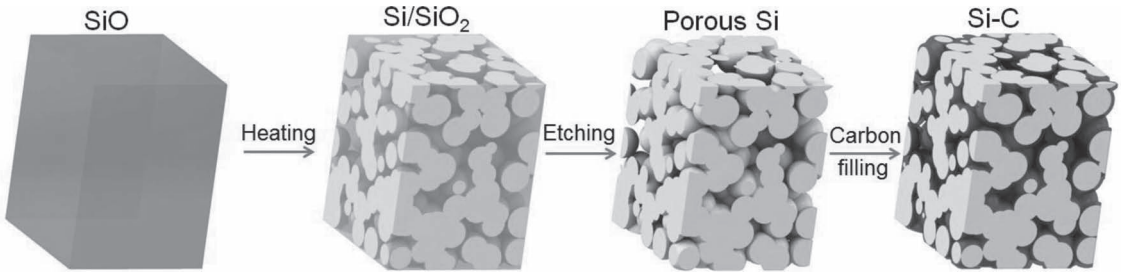

Figure 1. The preparation process from SiO precursor to the Si-C composite.

lithiation/delithiation process. It has been reported that Si nanoparticles with diameter less than 10 nm can sustain long cycling of lithiation/delithiation without observation of fracture.[31] 2) Si and C should be uniformly mixed at the nanoscale to improve the conductivity but also be highly packed to improve the tap density of the micro-sized particles. 3) The carbon and Si building blocks should maintain intimate contact even after the micro-sized Si-C particles are pulverized to prevent loss of electrical contact. Following this strategy, we report a new, low-cost, large-scale approach to prepare a micro-sized Si-C composite (US patent pending) with excellent performance as an anode material for LIBs. The composite shows a reversible capacity of 1459 mAh/g after 200 cycles at 1 A/g (97.8% capacity retention) and excellent high rate performance of 700 mAh/g at 12.8 A/g, and also has a high tap density of 0.78 g/cm^3. The excellent performance of the Si-C composite combined with its low-cost and large-scale synthesis makes it a promising anode material for practical application in LIBs.

The synthesis process of the Si-C composite is schematically summarized in **Figure 1**. Commercially available micro-sized SiO is employed as the Si source at a gram scale. The SiO is heated to form an Si/SiO_2 composite composed of interconnected Si nanoparticles embedded in an SiO_2 matrix due to the disproportionation of SiO.[32] This is followed by removal of the SiO_2 via an etching route, transforming the Si/SiO_2 composite into porous Si particles. Finally, carbon filling of a large portion of the original pores by thermal decomposition of acetylene creates a micro-sized Si-C composite in which Si and carbon are three-dimensionally interconnected at the nanoscale.

The phases of the precursors and products obtained at different steps in the synthesis process were characterized by X-ray diffraction (XRD). The SiO precursor shows two broad bumps in its XRD pattern (**Figure 2**a), indicating that it is amorphous. After treatment at 950 °C for 5 h, SiO disproportionates to crystalline Si (JCPDS Card No.27-1402 and space group Fd3m [227]) and amorphous SiO_2, as shown in Figure 2a. After the removal of SiO_2 by HF etching, a crystalline Si framework was obtained (Figure 2a). The broad Si peaks reveal that the as-obtained Si is composed of nanocrystallites with an average size of about 15 nm as estimated by the Debye–Scherrer equation. Raman spectroscopy confirms formation of Si and SiO_2 after disproportionation of SiO and the removal of SiO_2 after HF etching (Figure S1 in Supporting Information). X-ray photoelectron spectroscopy (XPS) (Figure 2b) shows the presence of Si and silicon oxides in the as-obtained material. A strong peak observed at 99.4 eV corresponds to the binding energy of Si(0).[10] A weak bump centered at around 103 eV suggests the presence of silicon oxides[27] that may be caused by the natural oxidation of the Si in air. After carbon deposition, the obtained Si-C composite shows a small bump between 20 and 25 degrees in its XRD pattern (Figure 2a), which is attributed to amorphous carbon. Raman spectroscopy (Figure 2c) shows two peaks at 1333 and 1614 cm^{-1} that correspond to the D (disordered) band and the G (graphite) band of carbon, respectively. The ratio of D to G band is estimated to be 2.3, confirming an amorphous carbon structure.[30] The mass percentage of carbon in the Si-C composite was found to be 20.8% by elemental analysis.

The morphology, size, and structure of the Si-C composite have been investigated by scanning electron microscopy (SEM) and transmission electron microscopy (TEM). SEM studies show that the Si-C composite is composed of micro-sized particles with average diameter of 20 μm (Figure 2d) and has similar morphology to SiO precursor powders (Figure S2 in Supporting Information). This suggests the microscale morphologies are maintained during the disproportionation, etching, and carbon deposition processes. TEM and high-resolution TEM (HRTEM) analyses reveal the structure of the Si-C composite at the nanoscale level. As shown in Figure 2e, the Si-C composite contains interconnected Si nanoparticles with a size of about 10 nm. The interconnected feature of Si is clearly exhibited in a high magnification TEM image (Figure S3 in Supporting Information). An HRTEM image (Figure 2f) taken on the edge of an individual composite particle shows many nanocrystallites in which lattice fringes with d-spacing of 3.1 Å are clearly distinguished, corresponding to the (111) crystal planes of the Si. Between these nanocrystallites, amorphous structures are observed and can be ascribed to the carbon. To examine the distribution of carbon in the Si-C composite particles, energy-dispersive X-ray spectroscopy (EDS) mapping was carried out on a cross section of a single Si-C composite particle, as shown in Figure 2g. The carbon was found to be uniformly distributed throughout the cross-section of the particle, indicating homogenous carbon filling. The distribution of carbon at nanoscale was also investigated by carbon mapping on a cross section of the Si-C composite using an energy-filtering TEM (EF-TEM). It can be clearly seen in Figure 2h and 2i that carbon is uniformly distributed among the interconnected Si nanoparticles. The results above demonstrate that micro-sized Si-C composite particles consist of nano-sized Si and C that are three-dimensionally interconnected at the nanoscale throughout the particles.

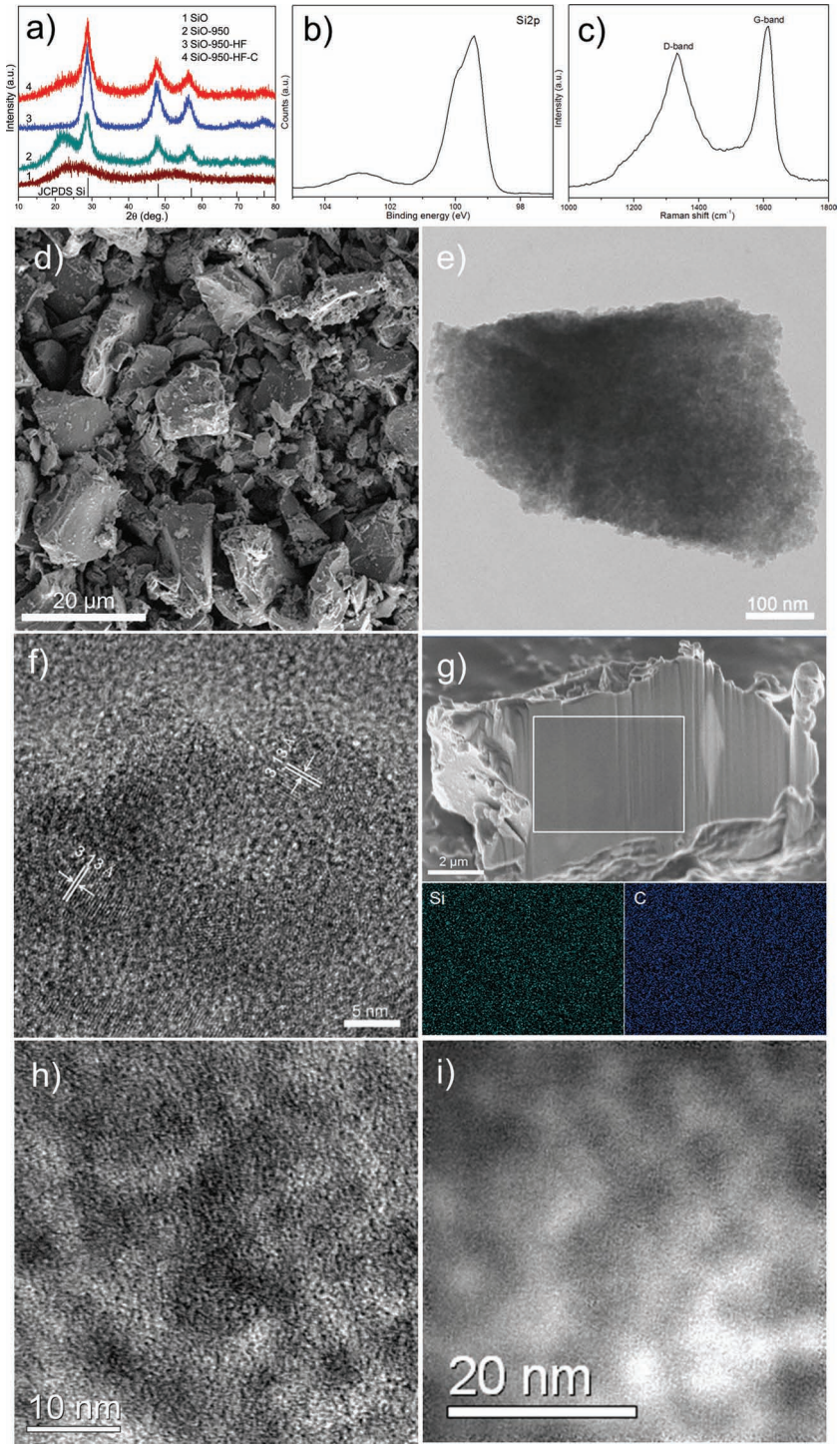

Figure 2. (a) XRD patterns of products obtained at different steps during preparation. (b) XPS spectrum of porous Si. (c) Raman spectrum, (d) SEM image, (e) TEM image, (f) HRTEM image, (g) cross-section SEM and EDS mapping of Si and C in the area marked by the white square, (h) HRTEM and (i) corresponding EF-TEM mapping of carbon in a cross-section of Si-C composite.

It has been well demonstrated that decreasing particle size to the nanoscale and/or introducing carbon can enhance the cycling stability and rate capability of Si-based anode materials.[9–18] Excellent electrochemical performance is thus expected for the Si-C composite. Electrochemical performance of the Si-C composite was characterized by galvanostatic charge/discharge in a coin-cell configuration. The voltage profiles of the Si-C composite and the porous Si without carbon filling at different charge/discharge cycles are shown in **Figure 3**a. The Si-C composite delivers initial discharge and charge capacities of 2004 and 1544 mAh/g at 400 mA/g, respectively, corresponding to a first cycle coulombic efficiency (CE) of 77%. In contrast, the porous Si has discharge and charge capacities of 1970 and 798 mAh/g, respectively, giving a low CE of only 40%. The improved first cycle CE is attributed to the lower specific surface area (87 m^2/g vs. 313 m^2/g of the porous Si) and stable SEI of the Si-C composite. Lower surface area leads to less side reaction on the Si surface and less irreversible consumption of Li.[33–35] The carbon filling can help to stabilize the formation of the SEI film.[36] The Si-C composite also has a higher specific capacity (1675 mAh/g) than the porous Si (1000 mAh/g) at 400 mA/g, as shown in Figure 3b. The capacity retention (based on the discharge capacity of the second cycle) of the Si-C composite is 96.6% after 50 cycles. The cyclic voltammetry (CV) curve of the first cycle of the Si-C composite is shown in Figure S4 in Supporting Information. The cathodic peaks below 0.2 V are ascribed to lithiation of Si and the anodic peak around 0.52V is attributed to lithium extraction from Si.[37] A very weak anodic peak around 0.3 V due to lithium extraction from SiO_x[37,38] is also present. This indicates that little SiO_x exists in the Si-C composite, which is consistent with the XPS result (Figure 2b). A capacity of 1459 mAh/g after 200 cycles at a higher current density of 1A/g and excellent capacity retention of 97.8% were also attained, with the first three cycles activated at 400 mA/g (Figure 3c). The excellent cycling stability is also reflected by the almost overlapped voltage profiles of the 4th and 203rd cycles (Figure 3a). The CE increases above 99.5% in 5 cycles and thereafter remains at that level. The Si-C composite also shows excellent high rate capability. As shown in Figure 3d, specific capacities of 1100 and 700 mAh/g can be achieved even at high current densities of 6.4 A/g and 12.8 A/g, almost 3 times and 2 times the theoretical capacity of graphite, respectively. The capacity recovers to 1630 mAh/g when the current rate is restored to the initial 400 mA/g, showing the composite's superior reversibility. The volumetric capacity of the micro-sized Si-C

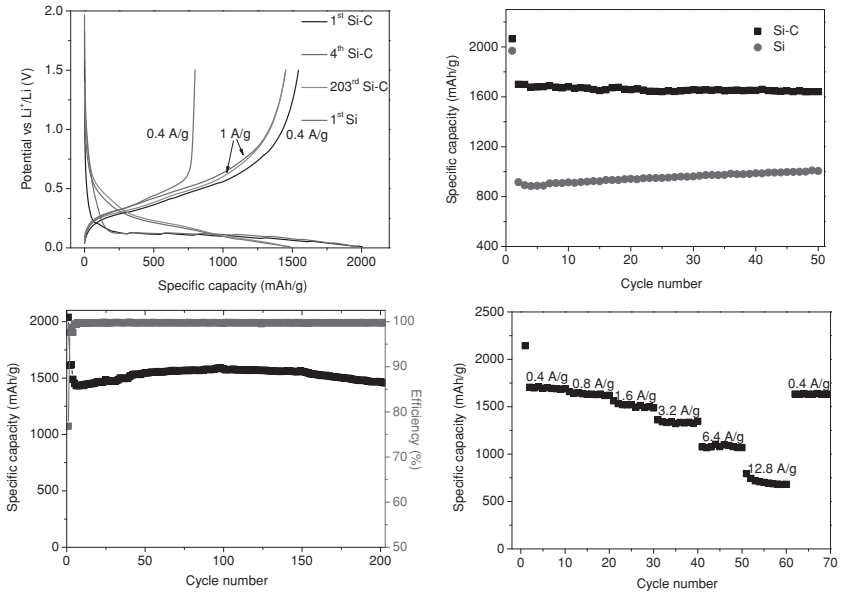

Figure 3. (a) Voltage profiles of the porous Si and Si-C composite. (b) Cycling performance of the porous Si and Si-C composite at 400 mA/g. (c) Long cycling performance of the Si-C composite at 1 A/g after first three cycles activated at 400 mA/g. (d) Rate performance of the Si-C composite.

composite is calculated (product of tap density and gravimetric specific capacity)[23,24] to be 1326 mAh/cm^3 at 400 mA/g. The high volumetric capacity is mainly due to the high tap density of the micro-sized Si-C composite (0.78 g/cm^3), which is higher than the reported porous C-Si nanocomposite (0.49 g/cm^3).[29]

Post-cycling SEM analyses show the morphology change of the Si-C composite electrode after charge/discharge to better understand the reason for such excellent cycling stability and rate performance of the micro-sized Si-C composite. Based on the thickness before (**Figure 4**a) and after lithiation (Figure 4b), the volume expansion of the Si-C composite electrode is calculated to be only 44%, similar to the reported result.[30] In addition, a uniform and crack-free film was observed on the top of Si-C composite, indicating a stable SEI layer on the Si-C composite electrode (Figure 4c). The SEM investigation on the electrode with the SEI layer removed also clearly demonstrates that the micro-sized Si-C composite particles (Figure S5 in Supporting Information) fragment into smaller particles during cycling, as shown in Figure 4d. However, the Si building blocks are still interconnected with carbon in the small particles, maintaining effective electrical contact and good utilization of silicon, as schematically illustrated by Figure 4e. To verify this point, a control electrode without using conductive carbon (i.e., Super P) was fabricated and evaluated, which would normally speed up capacity fading because of loss of electrical contact during cycling. The control electrode, however, exhibits similar first cycle CE (74%) and good capacity retention to the electrode with Super P at 1A/g (Figure S6 in Supporting Information). This result confirms that the micro-sized Si-C composite can maintain electrically-conducting pathways even after fracture and thus achieve excellent cycling stability. It should be noted that the conductive carbon additives are still needed to deliver high rate performance, where the electrical conductivity becomes the dominating limitation (Figure S7 in Supporting Information).

The excellent electrochemical performance of the micro-sized Si-C composite benefits from the nanoscale size of the Si building blocks and the uniform carbon filling. On the one hand, stress in nanoparticles can be easily relaxed without mechanical fracture. The small size also enables short transport pathways for both electrons and Li$^+$ ions, contributing to high rate capability. On the other hand, the uniform carbon filling offers three advantages. First, the carbon provides an effective physical buffer layer for the volume change of Si upon cycling, which preserves the structural integrity of the silicon building blocks. Second, the carbon filling forms an interpenetrating conductive network connecting the Si building blocks and thus improves the conductivity of the composite. Without carbon in intimate contact with silicon building blocks, electrons have to transport across the whole micro-sized particles to reach the nearest conductive carbon. In our case, the carbon filling forms a conductive network connecting each silicon building block and thus confines the electron transfer path to the nanoscale, which permits rapid charge and discharge. Third, the uniform carbon filling also ensures the maximum utilization of silicon even when the micro-sized particles break into small pieces upon cycling.

In summary, we have developed a facile route to produce a micro-sized Si-C composite composed of interconnected Si and carbon nanoscale building blocks. The Si-C composite exhibits a reversible capacity of 1459 mAh/g after 200 cycles at 1 A/g with a capacity retention of 97.8% and has a high tap density of 0.78 g/cm^3. Capacities of 1100 and 700 mAh/g can be obtained at high current densities of 6.4 A/g and 12.8 A/g, respectively. The excellent performance is attributed to the nanoscale size of primary particles and interconnected carbon and Si networks which can maintain internal electrical contact and sustain cycling stability. The synthesis method is low-cost and easy to scale up, and is thus believed to have great potential in practical production of high-performance Si materials for Li-ion batteries.

Experimental Section

Synthesis of the Si-C composite: Commercially available SiO powder (325 mesh) from Aldrich was used as the Si precursor. The disproportionation of SiO powder was carried out in a horizontal quartz tube. In a typical process, high-purity Ar was introduced at a flow rate of 1500 sccm for 20 min to purge the system. Afterwards the flow rate was reduced to 100 sccm and the tube was heated to 950 °C with a ramping rate of 10 °C/min and kept for 5 h. The samples were taken out of the tube at temperatures below 40 °C and immersed in 20 wt% HF solution (H_2O: ethanol = 5:1 by volume) at room temperature for 3 h to remove SiO_2. The obtained porous Si was collected by filtration and washed with distilled water and absolute ethanol in sequence several times. The final product was dried in a vacuum oven at 60 °C for 4 h. Carbon coating of

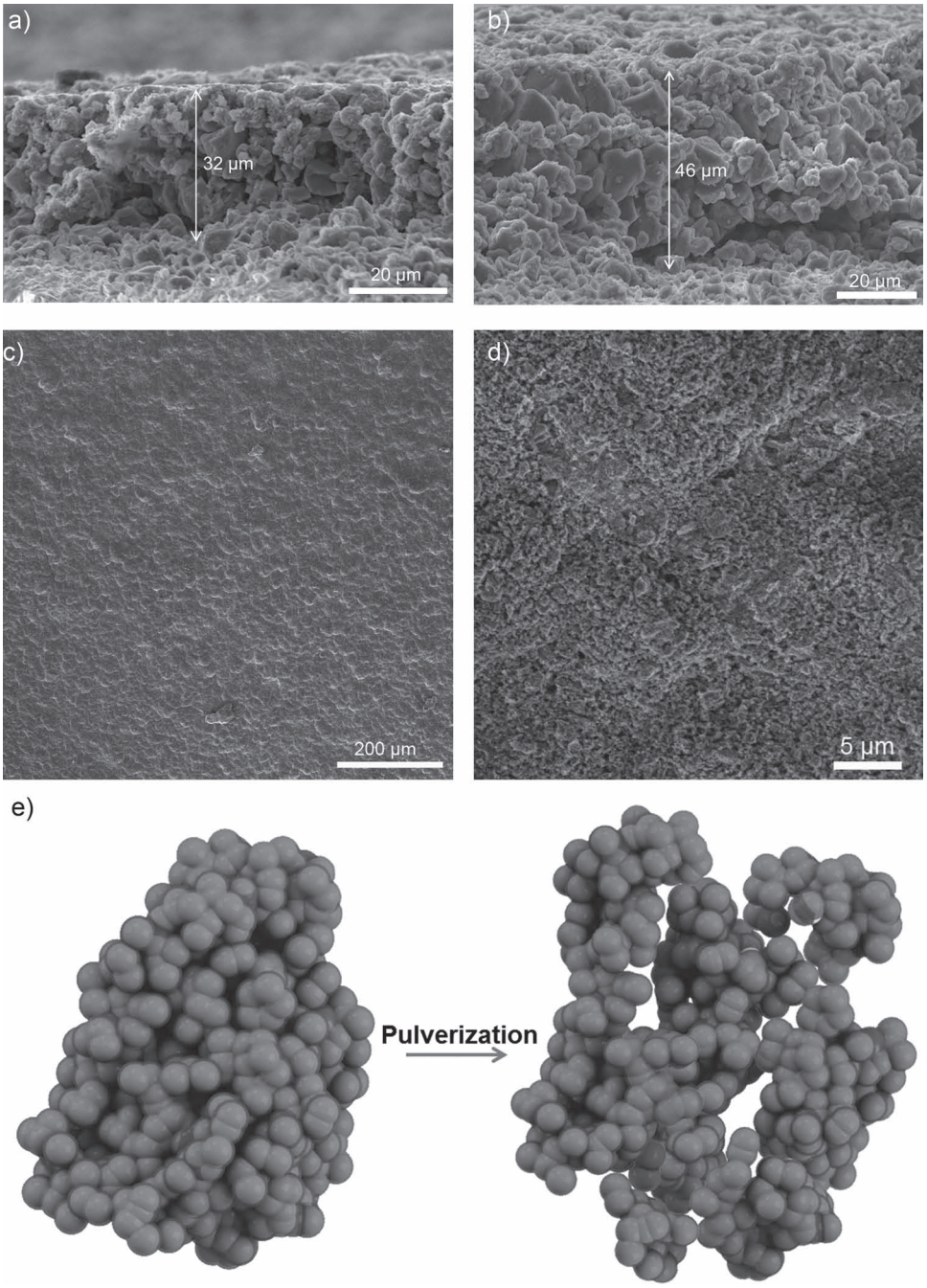

Figure 4. Cross-sectional SEM images of the Si-C composite electrode before (a) and after (b) lithiation at 400 mA/g. SEM images of SEI layer (c) and lithiated Si-C composite (d) after 10 cycles at 1 A/g. Schematic illustration (e) of the breaking process of the micro-sized Si-C composite during which the interconnected structure and electrical contact is maintained in broken parts.

porous Si was done by thermal decomposition of acetylene gas at 620 °C for 20 min in a quartz furnace. The mixture of acetylene and high-purity argon (argon: acetylene = 9:1 by volume) is introduced at a flow rate of 100 sccm.

Characterization: The obtained samples were characterized on a Rigaku Dmax-2000 X-ray powder diffractometer (XRD) with Cu Kα radiation (λ = 1.5418 Å). The operation voltage and current were kept at 40 kV and 30 mA, respectively. The size and morphology of the as-synthesized products were determined by a JEOL-1200 transmission electron microscope (TEM), FEI Nova NanoSEM 630 scanning electron microscope (SEM) and JEOL-2010F high-resolution transmission electron microscope (HRTEM). The Brunauer–Emmett–Teller (BET) specific surface area of the samples was determined by a Micrometrics ASAP 2020 physisorption analyzer using the standard N_2 adsorption and desorption isotherm measurements at 77 K. X-ray photoelectron spectroscopy (XPS) was conducted with a Kratos Analytical Axis Ultra XPS. Raman spectroscopy was conducted with a WITec CMR200 confocal Raman instrument.

Electrochemical measurements: The electrochemical experiments were performed using 2016-type coin cells, which were assembled in an

argon-filled dry glovebox (MBraun, Inc.) with the Si and carbon-coated Si electrode as the working electrode and the Li metal as the counter electrode. The working electrodes were prepared by casting the slurry consisting of 60 wt% of active material, 20 wt% of Super P carbon black, and 20 wt% of poly(acrylic acid) (PAA) binder. The mass loading of active materials is about 1.2 mg/cm^2 and the thickness of electrodes is about 30 µm. 1 mol/L $LiPF_6$ in a mixture of ethylene carbonate, diethyl carbonate and dimethyl carbonate (EC: DEC: DMC, 2:1:2 by vol.%) and 10 wt% fluoroethylene carbonate (FEC) was used as the electrolyte (Novolyte Technologies, Independence, OH). The electrochemical performance was evaluated by galvanostatic charge/discharge cycling on an Arbin BT-2000 battery tester at room temperature under different current densities in the voltage range between 1.5 and 0.01 V versus Li^+/Li. The current density and specific capacity are calculated based on the mass of carbon-coated Si composite.

Supporting Information

Support Information is available from the Wiley Online Library or from the author.

Acknowledgements

This work was supported by the Assistant Secretary for Energy Efficiency and Renewable Energy, Office of Vehicle Technologies of the U.S. Department of Energy under Contract No. DE-AC02-05CH11231, Subcontract NO. 6951378 under the Batteries for Advanced Transportation Technologies (BATT) Program.

Received: October 25, 2012
Revised: November 20, 2012
Published online: December 11, 2012

[1] A. S. Arico, P. Bruce, B. Scrosati, J. M. Tarascon, W. van Schalkwijk, *Nat. Mater.* **2005**, *4*, 366.
[2] M. Armand, J. M. Tarascon, *Nature* **2008**, *451*, 652.
[3] B. Kang, G. Ceder, *Nature* **2009**, *458*, 190.
[4] M. S. Whittingham, *Chem. Rev.* **2004**, *104*, 4271.
[5] M. Winter, J. O. Besenhard, M. E. Spahr, P. Novák, *Adv. Mater.* **1998**, *10*, 725.
[6] B. A. Boukamp, G. C. Lesh, R. A. Huggins, *J. Electrochem. Soc.* **1981**, *128*, 725.
[7] H. Wu, G. Chan, J. W. Choi, I. Ryu, Y. Yao, M. T. McDowell, S. W. Lee, A. Jackson, Y. Yang, L. Hu, Y. Cui, *Nat. Nano.* **2012**, *7*, 310.
[8] L. Y. Beaulieu, K. W. Eberman, R. L. Turner, L. J. Krause, J. R. Dahn, *Electrochem. Solid-State Lett.* **2001**, *4*, A137.
[9] H. Wu, G. Zheng, N. Liu, T. J. Carney, Y. Yang, Y. Cui, *Nano Lett.* **2012**, *12*, 904.
[10] N. Liu, H. Wu, M. T. McDowell, Y. Yao, C. Wang, Y. Cui, *Nano Lett.* **2012**, *12*, 3315.
[11] X. Li, P. Meduri, X. Chen, W. Qi, M. H. Engelhard, W. Xu, F. Ding, J. Xiao, W. Wang, C. Wang, J.-G. Zhang, J. Liu, *J. Mater. Chem.* **2012**, *22*, 11014.
[12] S. Chen, M. L. Gordin, R. Yi, G. Howlett, H. Sohn, D. Wang, *Phys. Chem. Chem. Phys.* **2012**, *14*, 12741.
[13] J. K. Yoo, J. Kim, Y. S. Jung, K. Kang, *Adv. Mater.* **2012**, *40*, 5452.
[14] M. Holzapfel, H. Buqa, W. Scheifele, P. Novák, F. M. Petrat, *Chem. Commun.* **2005**, 1566.
[15] J. K. Lee, K. B. Smith, C. M. Hayner, H. H. Kung, *Chem. Commun.* **2010**, *46*, 2025.
[16] L. F. Cui, Y. Yang, C. M. Hsu, Y. Cui, *Nano Lett.* **2009**, *9*, 3370.
[17] W. Zhou, S. Upreti, M. S. Whittingham, *Electrochem. Commun.* **2011**, *13*, 1102
[18] W. Wang, P. N. Kumta, *ACS Nano* **2010**, *4*, 2233.
[19] L. Su, Y. Jing, Z. Zhou, *Nanoscale* **2011**, *3*, 3967.
[20] C. K. Chan, H. Peng, G. Liu, K. McIlwrath, X. F. Zhang, R. A. Huggins, Y. Cui, *Nat. Nano.* **2008**, *3*, 31.
[21] X. Chen, K. Gerasopoulos, J. Guo, A. Brown, C. Wang, R. Ghodssi, J. N. Culver, *ACS Nano* **2010**, *4*, 5366.
[22] J. H. Warner, A. Hoshino, K. Yamamoto, R. D. Tilley, *Angew. Chem. Int. Ed.* **2005**, *44*, 4550.
[23] S. W. Oh, S. T. Myung, H. J. Bang, C. S. Yoon, K. Amine, Y.-K. Sun, *Electrochem. Solid-State Lett.* **2009**, *12*, A181.
[24] D. Applestone, A. Manthiram, *RSC Adv.* **2012**, *2*, 5411.
[25] J. H. Ryu, J. W. Kim, Y. E. Sung, S. M. Oh, *Electrochem. Solid-State Lett.* **2004**, *7*, A306.
[26] H. Kim, B. Han, J. Choo, J. Cho, *Angew. Chem. Int. Ed.* **2008**, *47*, 10151.
[27] B. M. Bang, J. I. Lee, H. Kim, J. Cho, S. Park, *Adv. Energy Mater.* **2012**, *2*, 878.
[28] B. M. Bang, H. Kim, H. K. Song, J. Cho, S. Park, *Energy Environ. Sci.* **2011**, *4*, 5013.
[29] A. Magasinski, P. Dixon, B. Hertzberg, A. Kvit, J. Ayala, G. Yushin, *Nat. Mater.* **2010**, *9*, 353.
[30] J. I. Lee, N. S. Choi, S. Park, *Energy Environ. Sci.* **2012**, *5*, 7878.
[31] H. Kim, M. Seo, M. H. Park, J. Cho, *Angew. Chem. Int. Ed.* **2010**, *49*, 2146.
[32] M. Mamiya, M. Kikuchi, H. Takei, *J. Cryst. Growth* **2002**, *237–239*, 1909.
[33] D. J. Xue, S. Xin, Y. Yan, K. C. Jiang, Y. X. Yin, Y. G. Guo, L. J. Wan, *J. Am. Chem. Soc.* **2012**, *134*, 2512.
[34] K. H. Seng, M. H. Park, Z. P. Guo, H. K. Liu, J. Cho, *Angew. Chem. Int. Ed.* **2012**, *51*, 5657.
[35] K. Evanoff, A. Magasinski, J. Yang, G. Yushin, *Adv. Energy Mater.* **2011**, *1*, 495.
[36] Y. C. Yen, S. C. Chao, H. C. Wu, N. L. Wu, *J. Electrochem. Soc.* **2009**, *156*, A95.
[37] T. Zhang, J. Gao, H. P. Zhang, L. C. Yang, Y. P. Wu, H. Q. Wu, *Electrochem. Commun.* **2007**, *9*, 886.
[38] Y. S. Hu, R. Demir-Cakan, M. Titirici, J. Muller, R. Schlogl, Markus Antonietti, J. Maier, *Angew. Chem. Int. Ed.* **2008**, *47*, 1645.